Biochimica et Biophysica Acta 1788 (2009) 724–731

Contents lists available at ScienceDirect

Biochimica et Biophysica Acta

journal homepage: www.elsevier.com/locate/bbamem

Atomic force microscopy differentiates discrete size distributions between membrane protein containing and empty nanolipoprotein particles

Craig D. Blanchette [a], Jenny A. Cappuccio [a], Edward A. Kuhn [a], Brent W. Segelke [a], W. Henry Benner [a], Brett A. Chromy [a], Matthew A. Coleman [a], Graham Bench [a], Paul D. Hoeprich [a,*], Todd A. Sulchek [b,*]

[a] Physical Life Sciences, Lawrence Livermore National Laboratory, Livermore, CA 94551, USA
[b] School of Mechanical Engineering, Georgia Institute of Technology, Atlanta, GA 30332, USA

ARTICLE INFO

Article history:
Received 3 October 2008
Received in revised form 11 November 2008
Accepted 14 November 2008
Available online 8 December 2008

Keywords:
Apolipoprotein
Nanolipoprotein particle
Nanodisc
Atomic force microscopy
Membrane protein
Bacteriorhodopsin
NLP

ABSTRACT

To better understand the incorporation of membrane proteins into discoidal nanolipoprotein particles (NLPs) we have used atomic force microscopy (AFM) to image and analyze NLPs assembled in the presence of bacteriorhodopsin (bR), lipoprotein E4 n-terminal 22k fragment scaffold and DMPC lipid. The self-assembly process produced two distinct NLP populations: those containing inserted bR (bR-NLPs) and those that did not (empty-NLPs). The bR-NLPs were distinguishable from empty-NLPs by an average increase in height of 1.0 nm as measured by AFM. Streptavidin binding to biotinylated bR confirmed that the original 1.0 nm height increase corresponds to br-NLP incorporation. AFM and ion mobility spectrometry (IMS) measurements suggest that NLP size did not vary around a single mean but instead there were several subpopulations, which were separated by discrete diameters. Interestingly, when bR was present during assembly the diameter distribution was shifted to larger particles and the larger particles had a greater likelihood of containing bR than smaller particles, suggesting that membrane proteins alter the mechanism of NLP assembly.

1. Introduction

Approximately one third of all eukaryotic proteins are membrane associated. These membrane proteins are involved in numerous vital biological processes including signal transduction, transport, adhesion, and cell–cell communication, and are the primary targets of many therapeutic drugs [1,2]. Despite the recognized importance of membrane proteins, few robust and versatile methods exist for the isolation and solubilization of these biological molecules in their properly folded and functional state. Self-assembling nanolipoprotein particles (NLPs) have been identified as a potential membrane mimetic for the solubilization of membrane proteins. Purified apolipoproteins and phospholipids are known to self-assemble in vitro to form nano-scale discoidal bilayer patches or NLPs, where the lipoproteins localize to the NLP perimeter [3–6]. Recently, it has been shown that when membrane proteins are present during the NLP self-assembly process, the membrane protein will associate with NLP constructs producing soluble and functional integral membrane protein complexes [7–17]. The ability to incorporate membrane proteins into the bilayer environment contained within the NLP offers both scientific and technological promise.

Although several groups have reported successful incorporation of membrane proteins into NLPs, their collective focus has been on characterization by PAGE analysis and functional assessment; quantification of overall yield and incorporation efficiency has largely been ignored. However, it will likely be important to understand and control membrane protein incorporation efficiencies and NLP heterogeneity in order to maximize the utility of NLPs for the study of membrane proteins.

Biochemical techniques along with single particle analyses can offer powerful insights into NLP size polydispersity [18–21] that may play an important role in understanding membrane protein incorporation. For example, atomic force microscopy (AFM) imaging, in principle, can directly verify incorporation of membrane proteins into individual NLPs, since the particle height resolution is sufficient to distinguish the topographic height change resulting from a membrane protein extending above the face of the phospholipid bilayer. Here, we use AFM to study bacteriorhodopsin incorporation into NLPs assembled from the phospholipid 1,2-Dimyristoyl-sn-Glycero-3-Phosphocholine (DMPC) and a fragment from the human apolipoprotein E4 (apoE422K).

2. Materials and methods

2.1. Materials

Phospholipid 1,2-Dimyristoyl-sn-Glycero-3-Phosphocholine (DMPC) was purchased from Avanti Polar Lipids, Inc. (Alabaster, AL). Bacteriorhodopsin was purchased from Sigma-Aldrich (St. Louis, MO).

* Corresponding authors. P. D. Hoeprich is to be contacted at Chemistry, Materials, Earth and Life Science, Lawrence Livermore National Laboratory, 7000 East Avenue, L-452, Livermore, CA 94550, USA. Tel.: +1 925 423 9298; fax: +1 925 422 2282. T.A. Sulchek, Georgia Institute of Technology, School of Mechanical Engineering, MRDC Building, 801 Ferst Drive, Atlanta, GA 30332, USA.
E-mail addresses: hoeprich2@llnl.gov (P.D. Hoeprich), todd.sulchek@me.gatech.edu (T.A. Sulchek).

0005-2736/$ – see front matter © 2008 Elsevier B.V. All rights reserved.
doi:10.1016/j.bbamem.2008.11.019

2.2. apoE422k protein production

The expression clone to produce apoE422k, the N-terminal 22 kDa fragment of apolipoprotein E4 (apoE4), as a 6-His and thioredoxin tagged construct was kindly provided by Dr. Karl Weisgraber. Production and purification of apoE422k have been described in detail elsewhere [6].

2.3. Nanolipoprotein particle (NLP) formation

bR-NLPs were assembled through a process adapted from the detergent dialysis technique [19]. The final concentration of detergent was above the critical micellar concentration. Sodium cholate (20 mM) was prepared from a 500 mM stock solution and added to DMPC suspended in Tris buffered saline to a concentration of 34 mg/ml and probe sonicated to clarity. The solution was briefly centrifuged to remove any metal contamination from the probe. Constituents were combined at the following concentrations; DMPC, 11 mM: apoE422k, 90.9 μM: bR, 49.8 μM; creating a molar ratio of 130:1:1.83 respectively. "Empty" NLPs (without bR) were assembled as described previously [6].

NLP assembly started with three repeated sets of transition temperature incubations, where the temperature was cycled from 30 °C for 10 min to 20 °C for 10 min, with gentle agitation between incubations. The reaction was incubated overnight at 23.8 °C. Cholate was removed by dialysis against 1000× volume of 10 mM Tris pH 7.4, 0.15 M sodium chloride, 0.25 mM EDTA, 0.005% sodium azide (TBS) buffer with 3 changes in 24 h. The NLPs were purified from free protein and free lipid by size-exclusion chromatography (VP HPLC, Shimadzu) using a Superdex 200 HR 10/30 column (GE Healthcare), in TBS at a flow rate of 0.5 ml/min. The column was calibrated with four protein standards of known molecular weight and Stokes diameter that span the separation range of the column and the NLP samples. The void volume was established with Blue dextran. Two fractions containing br-NLPs were concentrated to approximately 0.1 mg/ml using molecular weight sieve filters (Vivascience) with molecular weight cutoffs of 50 kDa. Protein concentration was determined using the ADV01 protein concentration kit (Cytoskeleton, Inc., Denver).

2.4. Fluorescent labeling

Cy3 and Cy2 were conjugated to the E422K scaffold and bR, respectively, using the Cy3/2 Ab Labeling Kit (GE Healthcare Life Sciences, Piscataway, NJ) as described in the manufacturer's instructions. Dye:protein ratios were determined by comparing the absorbance of the protein at 280 nm and the absorbance of the Cy dye at 670 nm and 532 nm respectively. In both cases, the ratios provided a 1:1 correlation, suggesting that on average a single Cy dye molecule is present on each protein.

2.5. Biotinylation

Bacteriorhodopsin in membrane sheets (Sigma) was selectively Biotinylated at solvent exposed lysines and primary amines using EZ-Link Sulfo-NHS-LC-Biotin (Pierce Chemical Co., Rockford, IL). There are 6 lysine residues and N terminal groups on the exposed cytosolic extracellular domains of bR. bR was resuspended in BupH PBS buffer pH 7.4 (Pierce). A freshly made 10 mM solution of EZ-Link Sulfo-NHS-LC-Biotin (Pierce) was prepared according to the manufactures recommendation in double-deionized H_2O (ddH_2O), added to the bR in a 20-fold molar excess and incubated on ice for 2 h. Excess biotin was removed by 3 repeated centrifugation steps in an ultracentrifuge at an 89,000 RCF for 20 min at 4 °C. The biotin labeled bR pellet was resuspended in TBS buffer. The percent recovery, by UV–visible spectroscopy, was determined to be 85–90% on average with careful re-suspension.

2.6. Microarray streptavidin binding

Proteins were spotted on GAPSII amino silane glass slides (Corning Life Sciences Inc., Corning, NY) in 4·4 squares with 16 replicates of each sample, generating ~300 μm diameter spots with a spot-to-spot distance of ~350 μm. All samples were spotted (10 nl) using a robotic system. Non-biotinylated bR and "empty"-NLPs served as the negative controls, and biotinylated bR served as the positive control. All samples containing bacteriorhodopsin had concentrations of 10 mM bR as determined by UV/vis spectroscopy, the NLP protein concentration without bR ("empty"-NLP) was 1.5 mg/ml. Proteins were cross-linked to the glass slides upon exposure to UV light for 5 min. An applied hybridization chamber (Grace Bio-labs, Bend, OR) was used for the blocking, washing and binding steps, with a volume capacity of 950 μl. Slides were blocked with BSA (1 mg/ml) for 30 min. Slides were washed with 1× PBS for 15 min followed by cyanine-5-streptavidin (Rockland Immunochemicals, Inc., Philadelphia, PA) binding (5 μg/ml) for 15 min. Subsequent washes were in 1× PBS and ddH_2O water each for 15 min. Slides were then dried by centrifugation. Cyanine 5-Streptavidin fluorescence in a ScanArray 5000 XL; PerkinElmer Proteins and NLPs were detected and imaged with a laser-based confocal scanner (ScanArray 5000 XL; PerkinElmer) using the VHeNe 594 nm laser for excitation of Cy5-labeled streptavidin. Images were collected and mean pixel intensities were analyzed using Scan Array software (Perkin Elmer Life and Analytical Sciences Inc., Waltham, MA).

2.7. Streptavidin binding for AFM

Streptavidin (SA) molecules (Sigma) were incubated with biotin-bR assembled NLPs (bio-br-NLPs) at a 2:1 molar ratio for 30 min and unbound SA was removed by filtering using molecular weight sieve filters (Vivascience) with molecular weight cutoffs of 100 kDa. The resultant particles were imaged by AFM.

2.8. Native PAGE

Equal amounts of NLP samples (0.5–2 μg) were diluted with 2× native sample buffer (Invitrogen Corps., Madison WI) and loaded onto 4–20% gradient pre-made Tris–HCl gels (Invitrogen). Samples were electrophoresed for 250 V h at a constant 125 V. After electrophoresis, gels were incubated with Sypro Ruby for 2 h and then destained using 10% MeOH and 7% Acetic acid. Following a brief wash with ddH_2O, gels were imaged using a Typhoon 9410 (GE Healthcare) at 532 nm (green laser) with a 610 nm bandpass 30 filter. Molecular weights were determined by comparing migration vs. log molecular weight of standard proteins found in the NativeMark standard (Invitrogen). The Stokes diameter of the NLPs was calculated from the known Stokes diameter of the same proteins in the standard sample.

2.9. SDS PAGE

Protein fractions were analyzed by SDS-PAGE gels, stained with Sypro Ruby (BioRad Laboratories, Inc., Hercules, CA) and fluorescently imaged with a Typhooon 9410 (GE Healthcare), as described above.

2.10. UV–visible spectroscopy

UV–visible spectra were collected using 50 μl of sample in a quartz cuvette on an ultrospec 5300pro UV/visible spectrophotometer (GE Healthcare) Dark adapted spectra were collected after keeping the sample wrapped in foil overnight. Light adapted spectra were collected after exposure to full spectrum bright light for 15 min.

2.11. AFM imaging

Atomically flat Muscovite mica disks were glued to metal substrates to secure them to the scanner of a stand-alone MFP-3D AFM (Asylum Research, Santa Barbara, CA). 2 μl of the NLP solution at a 100 ng/ml concentration was incubated for 2 min on the mica surface in imaging buffer (10 mM $MgCl_2$, 10 mM Tris–HCL, and 0.1 M NaCl, adjusted to pH 8.0) then lightly rinsed. The AFM has a closed loop in the *x*, *y*, and *z* axes, which improved imaging fidelity. The topographical images were obtained with oxide sharpened silicon nitride levers (MSCT, Veeco, Santa Barbara, CA) with a spring constant of 0.1 N/m. Images were taken in alternate contact (AC) mode, also known as tapping mode, in an aqueous environment, with amplitudes below 20 nm and an amplitude setpoint at 65% of the tapping amplitude, scan rates were below 1.5 Hz. Height, amplitude, and phase images were recorded. High resolution 600 nm by 600 nm images were acquired at 512 by 512 pixel resolution, such that each NLP on average contained 600 pixels. The density of particles on the mica substrate was kept low, on average 90 particles per 1 μm^2, to facilitate individual particle identification and sizing. Experiments were carried out in a temperature controlled room at 23±1 °C, with acoustic hood isolation and active vibration damping.

2.12. AFM image analysis

The height of features in the images were examined by histogram analysis using IgorPro Wavemetrics software routines, where contiguous particles were defined by a threshold height above the background and the height arbitrarily defined as the maximum height contained by 10 or more pixels within the particle. Particle diameter was determined by the full width half maximum (FWHM) analysis of contiguous particles in the slow scan direction (vertical), using IgorPro Wavemetrics software routines. In addition, to limit instrument broadening during lateral particle sizing, only tips revealing sharp imaging were used for diameter analysis. We have previously determined, based on NLP size and MD simulations, that the average tip broadening effect was ~2–3 nm [21]. To determine the reproducibility of the procedure used for measuring NLP diameters, randomly selected particles were repeatedly imaged to verify consistent diameter measurements. To remove image slopes and offsets, raw AFM images were flattened with a planar fit using Asylum Research data modification routines. To avoid coupling the NLP into the flattening procedure, surface features higher than 1 nm were masked followed by a second round of flattening. This procedure produced a flat mica surface while not altering the NLP height.

2.13. Ion mobility spectrometry

IMS determines the mean aerodynamic diameter population distribution of particles in a volatile buffer. NLP samples were exchanged via dialysis into a 25 mM ammonium acetate buffer and the aerodynamic diameter of NLPs were determined with a Macroion Mobility Spectrometer (Model 3890, TSI Inc., Shoreview, MN), as previously described [22,23]. NLP aerodynamic diameters were subsequently converted to aerodynamic spherical volumes as previously described [21].

3. Results

3.1. NLP assembly, SEC purification, native gel electrophoresis, SDS-PAGE analysis and UV–visible spectroscopy

Following assembly (Fig. 1A), NLPs were separated from other assembly components using SEC (Fig. 1B). The SEC profile contained four dominant peaks, a lipid rich peak, an NLP rich peak, apoE422k rich peak and bR rich peak (Fig. 1B). The NLPs from assemblies both in the absence and presence of bR were subjected to native-PAGE and SDS-PAGE electrophoresis (Fig. 2A and B). Bands on the native gel from the bR containing assemblies spanned the molecular weight range of 300–950 kDa, indicating the sample was highly heterogeneous. Single bands at ~22 kDa and ~21.5 kDa were observed by SDS-PAGE for empty NLP assemblies (lanes 2) and bR alone (lane 3), respectively (Fig. 2B). In contrast, NLPs assembled in the presence of bR (bR-NLP assembly—lane 4) contained two bands by SDS-PAGE at ~22 kDa and

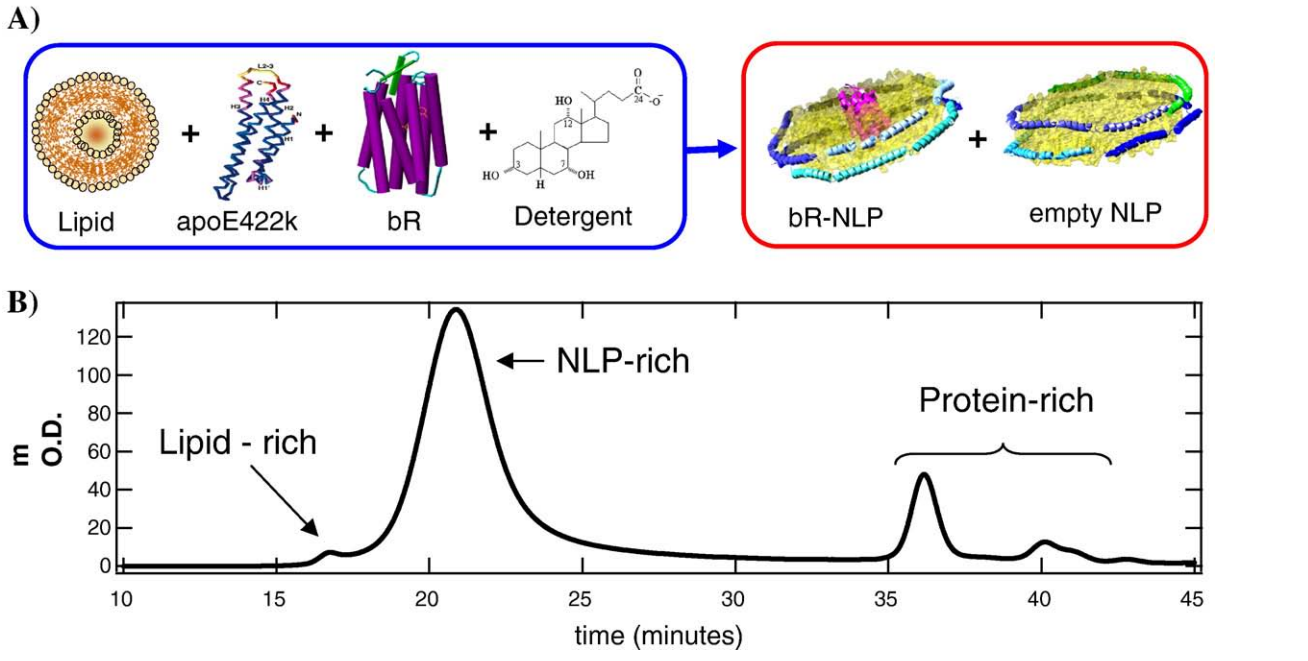

Fig. 1. (A) bR-NLP assembly protocol. The reagents undergo a temperature transition and detergent dialysis to self assemble the NLPs. (B) SEC chromatography purification after bR-NLP assembly monitored at absorbance of 280 nm. The SEC profile post NLP assembly contained four dominant peaks corresponding to (from left to right) a free lipid rich peak, an NLP rich peak, apoE422k rich peak and bR rich peak.

~21.5 kDa, indicating co-localization of these two proteins within the NLP constructs (Fig. 2B).

Native gels and SDS gels of SEC fractions from fluorescent assemblies were also imaged with a fluorescent scanner. Fluorescent scans of the native gel indicated that Cy3-E422k (red) and Cy2-bR (green) were in the same band (pseudo colored yellow) for SEC fractions spanning the entire NLP rich peak, again in the molecular weight range of 300–900 kDa (Fig. 2C). These results suggest that these two proteins are co-localized within the NLP constructs. Cy3-apoE422k and Cy2-bR bands were also observed by SDS-PAGE for bR-NLP assemblies in the SEC fractions that spanned the entire NLP rich peak. Interestingly, early eluting fractions (lane 4) appeared to contain a higher concentration of Cy2-bR relative to Cy3-apoE422k (Fig. 2D).

To assess the functional state of bacteriorhodopsin after br-NLP assembly UV–visible spectroscopy of light- and dark-adapted br-NLPs was conducted. A 6 nm red-shift between the dark and light adapted spectra, from 550.7 nm to 556.0 nm peak, was observed by this technique (Fig. 2E). This shift indicates a properly folded protein structure [24]. In addition, the NLP solution was purple indicating bound retinal (data not shown).

3.2. Atomic Force Microscopy (AFM) and Ion mobility spectrometry (IMS) analysis of NLPs

Fig. 3A shows a typical 600 nm×600 nm AFM image of NLPs from a bR-NLP assembly that have been adsorbed onto a mica surface; the inset provides a more detailed perspective of two NLPs. AFM images were pseudo colored where red represents the mica surface and green represents the tops of NLPs (Fig. 3A). NLP height and full width at half maximum (FWHM) diameter was determined through cross-sectional analysis as demonstrated in Fig. 3B. Height and diameter data was used to establish height versus diameter scatter plots of NLPs assembled in both the presence (bR-NLP assembly) and absence (empty NLP assembly) of bR (Fig. 3C). These scatter plots show two discernible populations of NLPs in the br-NLP assembly, those with heights that are consistent with NLP heights from an empty-NLP reaction and a population of particles with heights that significantly exceed those of empty particles. Empty NLPs had an average height of 4.5 nm corresponding closely to empty-NLP heights measured previously [6,21] and to known DMPC phospholipid bilayer thickness [25,26]. The particles with increased height in the br-NLP assembly

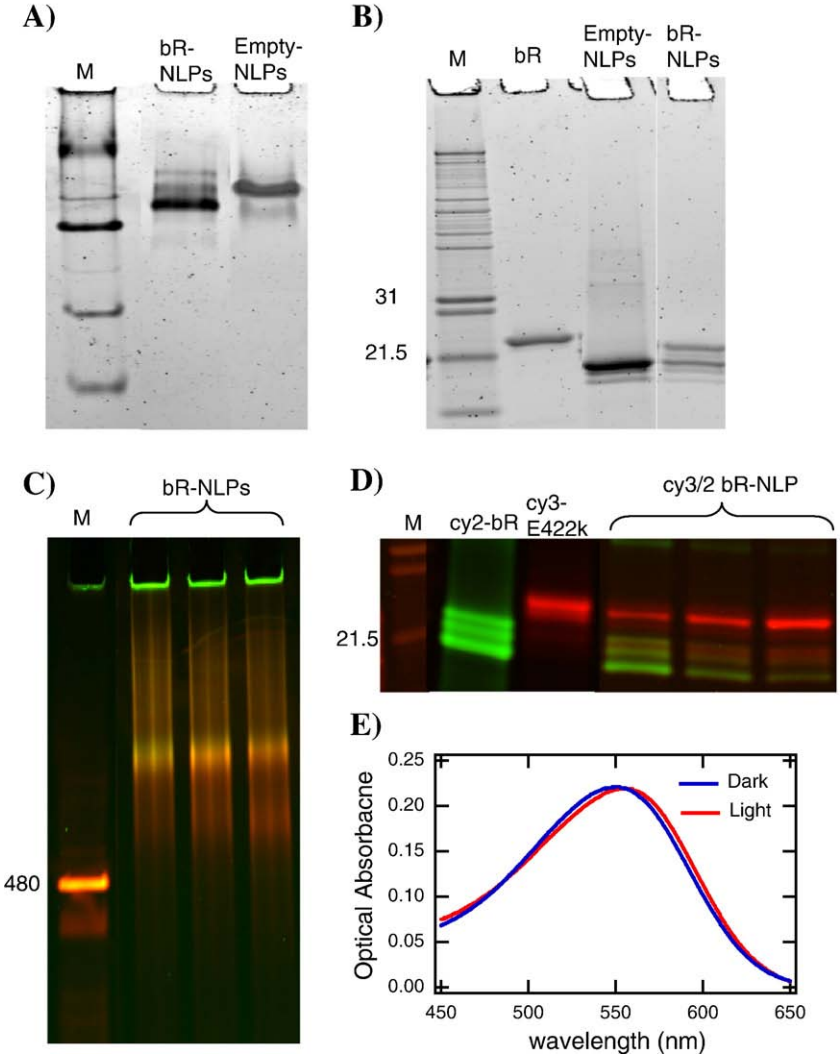

Fig. 2. Native gel, SDS PAGE and UV—visible spectroscopy of bR-NLPs. (A) Native gel electorphoresis of bR-NLPs and empty-NLPs. (B) Tricine denaturing gel 16% SDS PAGE for an empty-NLP assembly, bR, and bR-NLP assembly. The bR-NLP lane displays two distinct bands corresponding to bR and apoE422k. (C) Native gel electrophoresis of 3 SEC fractions spanning the entire NLP-rich peak for bR-NLPs assembled from cy2 labeled bR and cy3 labeled apoE422k, where green indicates cy3-E422k, red indicates cy2-bR and the yellow is the co-localization of both proteins. In the marker lane the 480 kDa and 720 kDa MW bands were based on a sypro stain of the gel. (D) Tricine denaturing gel 16% SDS PAGE of Cy2-bR, Cy3-apoE422k and 3 SEC fractions spanning the entire NLP-rich peak for bR-NLPs assembled from Cy2-bR and Cy3-apoE422k. The Cy3/Cy2 bR-NLPs contained two bands; a red band and green band indicating the presence of both cy2-bR and cy3-apoE422k. E) UV–vis absorbance spectra showing 550.7 nm and 556.0 nm absorbance maxima for dark adapted bR-NLPs and light adapted bR NLPs respectively. Empty NLPs showed no significant absorbance at these wavelengths (not shown).

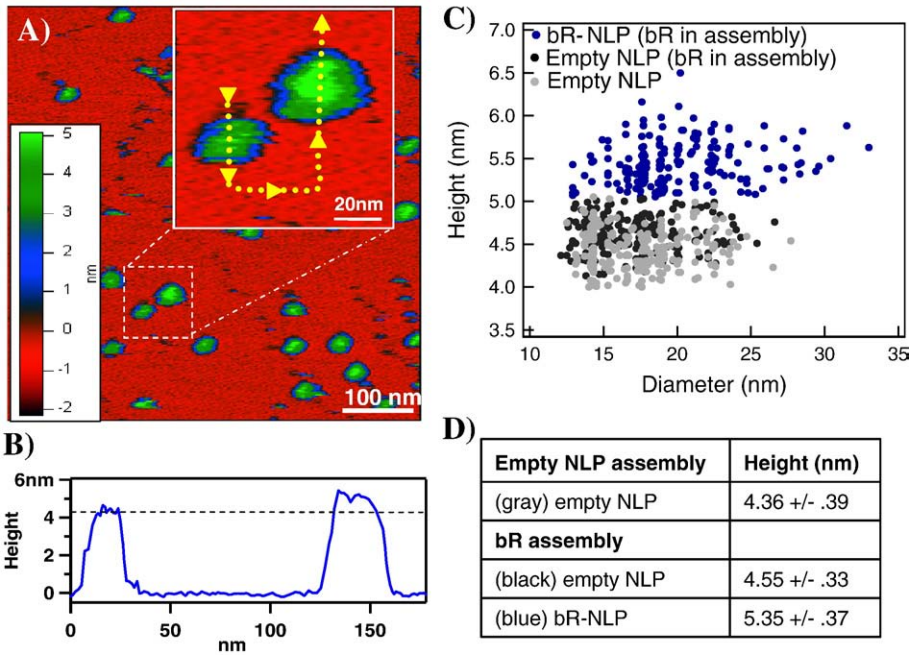

Empty NLP assembly	Height (nm)
(gray) empty NLP	4.36 +/- .39
bR assembly	
(black) empty NLP	4.55 +/- .33
(blue) bR-NLP	5.35 +/- .37

Fig. 3. AFM (A) AFM image of NLPs from a bR assembly showing particles with and without bR association (inset zoom with 20 nm scale bar). (B) Cross-sectional height of particles. Cross-section is indicated by the yellow dotted line in the image inset. Arrows indicate the direction of the cross-section. (C) Scatter plots showing individual particle height and FWHM diameter for both an empty assembly with no bR added, and an assembly with bR. (D) Average height and standard deviation calculated from scatter plots in C.

had an average height of 5.4 nm, an increase of approximately 1 nm over those of empty NLPs. Such heights correspond to the height difference determined for bR embedded in liposomes by AFM [27] and is consistent with dimensions and spatial orientation observed in the bR crystal structure [28].

From this analysis, particles with heights greater than two standard deviations above the average height of NLPs assembled in the absence of bR were designated by blue dots in Fig. 3C, while those with height values below this cutoff were designated by black dots in Fig. 3C. Fig. 3D summarizes the height change observed when comparing br-NLPs to empty-NLPs. Increases in height were consistent with bR association and insertion into the NLPs with overall yields corresponding to 50–70% bR-NLPs.

Protein microarrays were used to verify successful biotinylation of bR through binding of Cy5-labeled streptavidin to biotinylated bR and biotinylated br-NLPs (Fig. 4A–D). Fluorescence scanning of the protein arrays showed a 4.7 fold increase in fluorescence with biotinylated bR (p-value of 2.37×10^{-05}) relative to the non-biotinylated control, compared to a 5.6 fold increase for bR-NLPs (p-value of 6.29×10^{-12}) relative to the non biotinylated control indicating proper biotinylation of bR.

AFM imaging and height analysis of the biotin br-NLP assembly before streptavidin (SA) addition, revealed a bimodal height distribution (centered at 4.4±0.3 nm and 5.4±0.3 nm) as described above. After streptavidin addition a notable increase in height was observed for a sub-population of particles indicating that SA bound selectively to biotin-br-NLPs. A representative image and cross-section is shown in Fig. 4E–F. Several particles, identified by white pseudo color, were greater than 6 nm in height clearly identifying topographic enhancement of the particles. The cross-sectional line trace in Fig. 4F shows particle heights ranging from 4.2 nm to 9.8 nm. A histogram analysis of several hundred NLP heights revealed that the peak corresponding to a height centered at 5.4 nm before SA addition was markedly reduced following SA addition and replaced with a population of particles of increased heights (Table 1). These taller particles had a broad height distribution spanning 6.2 nm to 11 nm, consistent with subunit or tetrameric streptavidin bound to biotinlyated br-NLPs [29]. Non-biotinylated br-NLPs showed no significant increase in overall height with SA addition (Table 1). It is worth noting that we observed a relative increase in the fraction of empty-NLPs (i.e. NLPs with heights between 4.0 and 5.0 nm) after SA incubation. We currently do not know why this occurred but it may have been due to the spin filtration

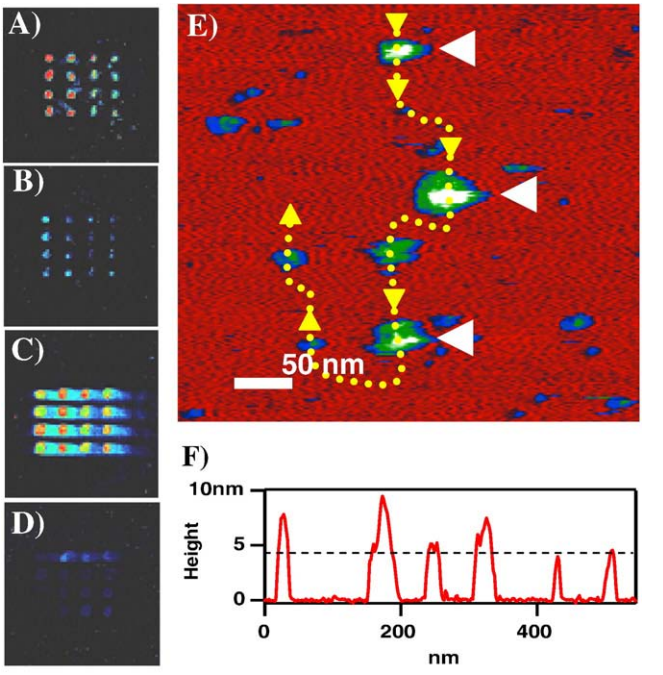

Fig. 4. Data showing biotinylated-bR NLPs binding to streptavidin (SA). (A–D) shows microarray binding data for Cy5 labeled SA binding to the following reagents: A) positive control, biotinylated bR, (B) negative control, non-biotinylated bR, (C) biotin bR-NLPs, and (D) empty-NLPs. (E) AFM image of biotin-bR NLPs incubated with SA, then immobilized on mica substrate. White color represents height of 7–10 nm. (F) Height section plot of path outlined by the yellow dotted line in the image. Arrows indicate the direction of the cross-section.

Table 1
Particle height data for biotin-bR NLPs and bR-NLPs before and after the incubation of SA

Condition	4.0–5.0 nm	5.0–6.0 nm	>6.0 nm
Biotin bR-NLP/ −SA	0.46	0.54	0
Biotin bR-NLP/ +SA	0.61	0.05	0.34
bR-NLP/ −SA	0.45	0.53	0.02
bR-NLP/ +SA	0.61	0.39	0

step that was done after the particles were incubated with SA to separate NLPs from unbound SA. Therefore, it is possible that some material was lost during this process, which may account for the relative increase in the population of empty-NLPs. Despite this discrepancy, after SA addition almost no NLPs displayed a height between 5.0 and 6.0 nm, which support the notion that the NLPs with 5.0–6.0 nm heights represented bR containing NLPs.

Diameters determined by AFM for NLPs assembled both in the presence and absence of bR did not vary around a single mean but rather varied slightly around several discrete and stable means (Fig. 5A). The existence of discrete NLP diameters is consistent with our previous report where NLP size distributions were quantified [21]. The diameter histogram determined by AFM clearly indicates that the diameter distribution shifts to larger particle sizes for NLPs assembled in the presence of bR (Fig. 5A). To verify the observed shift in the diameter distribution for particles assembled in the presence of bR, particle sizes were also analyzed by ion mobility spectrometry (IMS). The IMS traces confirms that the diameter distribution is shifted to larger particles for NLPs assembled in the presence of bR (black line) relative to empty NLP assemblies (gray line) (Inset, Fig. 5A). NLPs from the control assembly (not containing bR) (Fig. 5A — gray line) and NLPs from bR-NLP assemblies whose height was similar to that of NLPs assembled in the absence of bR (Fig. 5B — black line) were more likely to have diameter values of 18 nm and smaller. However, NLPs from the bR-NLP assemblies whose height is 1 nm larger than that of NLPs assembled in the absence of bR are more likely to have diameters of 18 nm and larger (Fig. 5B — blue line).

4. Discussion

AFM has previously been used to accurately discriminate two subpopulations of particles [30–32]. In this study, AFM was used as a single particle imaging technique and a significant increase in height for a relatively large fraction of NLPs assembled with bR was observed. Since empty NLPs rarely attain heights above 5 nm we hypothesize that the larger height values in the bR assembly resulted from an incorporated bR. If we assume the height distribution of br-NLPs and empty-NLPs within the same sample are described by two Gaussian distributions, we find the first is centered at 4.6 nm ± 0.3 nm and the second centered at 5.4 nm ± 0.4 nm. These two population peaks are separated by 0.8 nm, which corresponds closely to the height differential of a bR molecule [27] and the phospholipid bilayer [26].

To further verify identification of successful bR incorporation we assembled NLPs in the presence of biotinylated bR. Biotinylation of bR and the association of biotin-bR with NLPs were confirmed by visualizing binding of Cyanine 5 (Cy5) labeled streptavidin in protein microarrays. It was also shown that streptavidin did not significantly bind to empty-NLPs prepared in the absence of bR. Because our microarray data could not distinguish between br-NLPs and empty-NLPs within the same sample, we utilized streptavidin binding as a molecular contrast agent to selectively identify individual br-NLPs. This is equivalent to improving image contrast in optical microscopy by adding a dye contrast agent. Similar approaches have been used previously in AFM imaging [32]. By binding streptavidin, the topographic height differential between br-NLPs and empty NLPs within a given sample increased from less than 1 nm to over 2.5 nm. This method for identifying membrane proteins within NLPs is

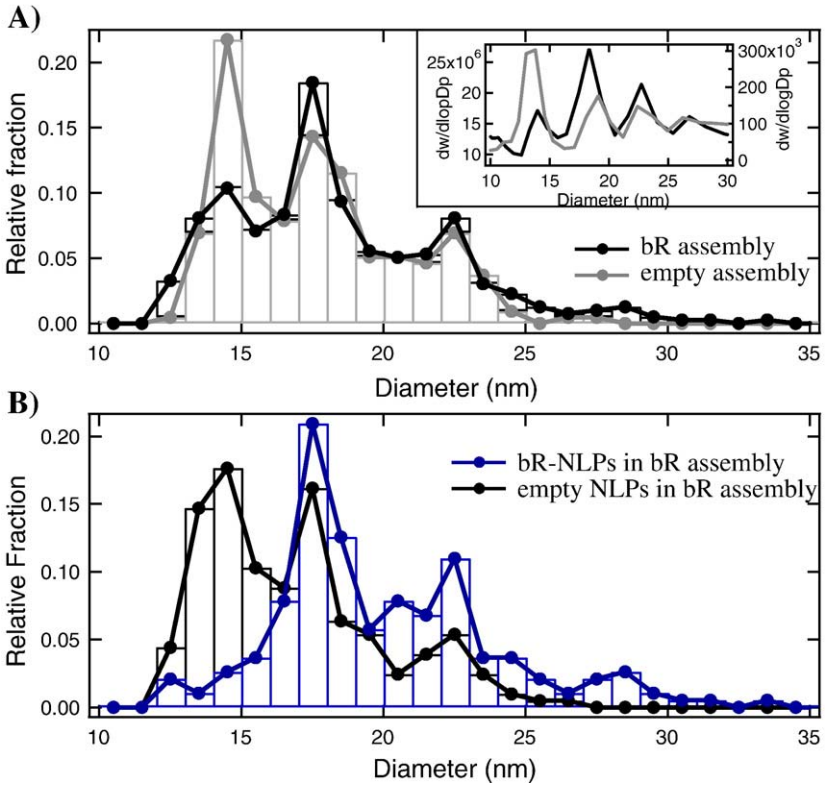

Fig. 5. (A) Histogram of NLP diameter determined through AFM for the bR assembly (black line) and empty control assembly (gray line). Inset — IMS traces of particle diameter distribution for the bR assembly (black line) and empty control assembly (gray line). (B) Diameter distributions for bR-NLPs (blue line) and empty NLPs (black line) in the bR assembly.

Table 2
The fraction of NLPs containing bR for a given NLP size

NLP diameter	Fraction bR
14+/−2	0.26
17+/−2	0.62
22+/−2	0.7
28+/−2	0.79
33+/−2	1

applicable to other membrane protein systems through biotinylation and binding of streptavidin or by using antibodies specific to the membrane protein. Through this combined approach we were able to determine that approximately 60% of the NLPs contained bR under these assembly conditions.

The ability to identify whether individual particles incorporate bR allowed us to correlate NLP diameter and bR incorporation. The empty- and br-containing NLPs show diameters with discrete and stable diameters [21], with the caveat being that the br-NLP diameter distributions were shifted to larger values relative to empty-NLPs (Fig. 5A and B) The empty-NLP distribution in the samples assembled in the presence and absence of bR was skewed toward the smallest diameter NLP (14 nm). In contrast, the proportion of the smallest diameter particles in bR-NLPS significantly reduced and the proportion of larger particles at 18 nm, 23 nm, and 28 nm greatly increased. Not only were br-NLPs larger on average than the empty-NLPs, but the presence of bR during self-assembly appears to drive the formation of larger diameter particles (Fig. 5A). It is worth noting that molecular modeling and simulations suggest that the discrete stable diameters observed here are consistent with discrete numbers of apolipoprotein scaffolding stabilizing the circumference of different particle sizes.

To quantify this effect, the fraction of bR containing NLPs was calculated for each discrete size. This value was calculated as the ratio of br-NLPs to the sum of NLPs within a diameter range determined from the peaks of Fig. 5B. These values as a function of particle diameter are listed in Table 2. The incorporation probability correlated closely with particle diameter; it was lowest for the smallest particles from peak 1 (less than 26%) and increased to 100% for particles larger than 30 nm.

It is not clear why the presence of bR results in the formation of larger particles. The likely form of incorporated bR was a monomer (22 kDa) or trimer (66 kDa) depending upon the lipid:bR stoichiometry [16]. Spectral results from the light/dark adaptation show absorption maxima (550.7 nm/556.0 nm) that are in between that of detergent solubilized monomeric (546 nm/553 nm) and trimeric (560 nm/568 nm) bR, respectively [24]. The larger trimer with associated archaeal lipid has a crossectional area of 3380 A^2 in the plane of the lipid bilayer [33] and has a diameter that is less than 8 nm [34] and thus should readily fit into 14 nm particles. That this rarely occurs can perhaps be explained by the fact that physiological lipids surrounding the bR may be carried through the purification and assembly process by tight binding [28] or that the some amount of DMPC lipid is utilized in the self assembly. Alternatively, bR-NLPs may contain bR oligomers that are larger than a trimer.

Our results show that the membrane protein bR was not incorporated into every NLP. However, the incorporation probability may be improved by assembling the NLP under conditions that favor the formation of larger particles. Previous investigations have measured bR-NLPs with a truncated apoA scaffold to be 9.2 nm in diameter as determined by calibrated size exclusion chromatography [17]. However, this method measures an average of all species in a mixture; thus it is not suitable for observing multiple particle sizes. In fact, heterogeneous particles were observed by TEM imaging, however the authors of this study did not focus on NLP size distribution [17]. Furthermore, the efficiency of bR incorporation was not quantified so it is possible that the majority of particles displaying bR activity were larger than the reported 9.2 nm. In fact by using larger scaffold proteins and smaller lipid to bR ratios, Bayburt et al. recently showed that larger particles contain a higher fraction of trimer versus monomer bR species [16], which may also reflect higher efficiencies of bR incorporation. It is also worth noting that NLPs were assembled with DMPC, which is not a typical lipid found in cellular membranes. Therefore, it is plausible that the use of native lipids for NLP assembly may increase the membrane protein incorporation efficiency, since the native lipid–membrane protein interactions may be more favorable than DMPC–membrane protein interactions. Based on this notion, it would be valuable to examine the effects of the lipid component on membrane protein incorporation efficiencies, particularly when this technology is utilized for the solubilization of a wider range of membrane proteins.

We have demonstrated methods to quantify NLP membrane protein incorporation efficiencies and have shown that the levels of incorporation vary with NLP size. The most significant and novel result was that larger particles had a greater likelihood of containing bR than smaller particles. These results may prove valuable for future strategies in designing protocols for membrane protein incorporation. It has been shown that the size of empty NLPs can be controlled by the use of different sized scaffolds or by changing the ratios of protein to lipid [18,35]. Therefore, future strategies may involve engineering scaffold proteins to form larger particles in combination with utilizing protein to lipid ratios that drive the NLP assembly process to larger particles.

Acknowledgments

This work was performed under the auspices of the U.S. Department of Energy by Lawrence Livermore National Laboratory under Contract DE-AC52-07NA27344 with support from Lawrence Livermore National Laboratory (LDRD 06-SI-003 awarded to PDH). UCRL-JRNL-235806.

References

[1] J. Drews, Drug discovery: a historical perspective, Science 287 (2000) 1960–1964.
[2] E. Wallin, G. von Heijne, Genome-wide analysis of integral membrane proteins from eubacterial, archaean, and eukaryotic organisms, Protein Sci. 7 (1998) 1029–1038.
[3] A. Jonas, S.M. Drengler, B.W. Patterson, 2 types of complexes formed by the Interaction of apolipoprotein a-I with vesicles of L-alpha-dimyristoylphosphatidylcholine, J. Biol. Chem. 255 (1980) 2183–2189.
[4] B. Lu, J.A. Morrow, K.H. Weisgraber, Conformational reorganization of the four-helix bundle of human apolipoprotein E in binding to phospholipid, J. Biol. Chem. 275 (2000) 20775–20781.
[5] M. Wientzek, C.M. Kay, K. Oikawa, R.O. Ryan, Binding of insect apolipophorin-Iii to dimyristoylphosphatidylcholine vesicles — evidence for a conformational change, J. Biol. Chem. 269 (1994) 4605–4612.
[6] B.A. Chromy, E. Arroyo, C.D. Blanchette, G. Bench, H. Benner, J.A. Cappuccio, M.A. Coleman, P.T. Henderson, A.K. Hinz, E.A. Kuhn, J.B. Pesavento, B.W. Segelke, T.A. Sulchek, T. Tarasow, V.L. Walsworth, P.D. Hoeprich, Different apolipoproteins impact nanolipoprotein particle formation, J. Am. Chem. Soc. 129 (2007) 14348–14354.
[7] T.H. Bayburt, J.W. Carlson, S.G. Sligar, Reconstitution and imaging of a membrane protein in a nanometer-size phospholipid bilayer, J. Struct. Biol. 123 (1998) 37–44.
[8] T.H. Bayburt, A.J. Leitz, G. Xie, D.D. Oprian, S.G. Sligar, Transducin activation by nanoscale lipid bilayers containing one and two rhodopsins, J. Biol. Chem. 282 (2007) 14875–14881.
[9] T.H. Bayburt, S.G. Sligar, Single-molecule height measurements on microsomal cytochrome P450 in nanometer-scale phospholipid bilayer disks, Proc. Natl. Acad. Sci. U. S. A. 99 (2002) 6725–6730.
[10] T. Boldog, S. Grimme, M.S. Li, S.G. Sligar, G.L. Hazelbauer, Nanodiscs separate chemoreceptor oligomeric states and reveal their signaling properties, Proc. Natl. Acad. Sci. U. S. A. 103 (2006) 11509–11514.
[11] T. Boldog, M. Li, G.L. Hazelbauer, Using nanodiscs to create water-soluble transmembrane chemoreceptors inserted in lipid bilayers, Methods Enzymol. 423 (2007) 317–335.
[12] F. Cruz, D.E. Edmondson, Kinetic properties of recombinant MAO-A on incorporation into phospholipid nanodisks, J. Neural Transm. 114 (2007) 699–702.
[13] A.J. Leitz, T.H. Bayburt, A.N. Barnakov, B.A. Springer, S.G. Sligar, Functional reconstitution of Beta2-adrenergic receptors utilizing self-assembling Nanodisc technology, Biotechniques 40 (2006) 601–602, 604, 606.
[14] M.R. Whorton, M.P. Bokoch, S.G.F. Rasmussen, B. Huang, R.N. Zare, B. Kobilka, R.K. Sunahara, A monomeric G protein-coupled receptor isolated in a high-density

lipoprotein particle efficiently activates its G protein, Proc. Natl. Acad. Sci. U. S. A. 104 (2007) 7682–7687.
[15] M.R. Whorton, B. Jastrzebska, P.S. Park, D. Fotiadis, A. Engel, K. Palczewski, R.K. Sunahara, Efficient coupling of transducin to monomeric rhodopsin in a phospholipid bilayer, J. Biol. Chem. 283 (2008) 4387–4394.
[16] T.H. Bayburt, Y.V. Grinkova, S.G. Sligar, Assembly of single bacteriorhodopsin trimers in bilayer nanodiscs, Arch. Biochem. Biophys. 450 (2006) 215–222.
[17] T.H. Bayburt, S.G. Sligar, Self-assembly of single integral membrane proteins into soluble nanoscale phospholipid bilayers, Protein Sci. 12 (2003) 2476–2481.
[18] A. Jonas, Reconstitution of high-density lipoproteins, Methods Enzymol. 128 (1986) 553–582.
[19] A. Jonas, K.E. Kezdy, J.H. Wald, Defined apolipoprotein A–I conformations in reconstituted high density lipoprotein discs, J. Biol. Chem. 264 (1989) 4818–4824.
[20] C.D. Mitchell, W.C. King, K.R. Applegate, T. Forte, J.A. Glomset, K.R. Norum, E. Gjone, Characterization of apolipoprotein E-rich high-density lipoproteins in familial lecithin–cholesterol acyltransferase deficiency, J. Lipid Res. 21 (1980) 625–634.
[21] C.D. Blanchette, L. Richard, W.H. Benner, J.B. Pesavento, J.A. Cappuccio, V.L. Walsworth, E.A. Kuhn, M. Corzett, B.A. Chromy, B.W. Segelke, M.A. Coleman, G. Bench, P.D. Hoeprich Jr., T.A. Sulchek, Quantifying size distributions of nanolipoprotein particles (NLPs) with single particle analysis and molecular dynamic (MD) simulations, J. Lipid Res. 49 (2008) 1420–1430.
[22] G. Bacher, R. Korner, A. Atrih, S.J. Foster, P. Roepstorff, G. Allmaier, Negative and positive ion matrix-assisted laser desorption/ionization time-of-flight mass spectrometry and positive ion nano-electrospray ionization quadrupole ion trap mass spectrometry of peptidoglycan fragments isolated from various bacillus species, J. Mass Spectrom. 36 (2001) 124–139.
[23] J.A. Loo, B. Berhane, C.S. Kaddis, K.M. Wooding, Y. Xie, S.L. Kaufman, I.V. Chernushevich, Electrospray ionization mass spectrometry and ion mobility analysis of the 20S proteasome complex, J. Am. Soc. Mass Spectrom. 16 (2005) 998–1008.
[24] J. Wang, S. Link, C.D. Heyes, M.A. El-Sayed, Comparison of the dynamics of the primary events of bacteriorhodopsin in its trimeric and monomeric states, Biophys. J. 83 (2002) 1557–1566.
[25] A.F. Xie, R. Yamada, A.A. Gewirth, S. Granick, Materials science of the gel to fluid phase transition in a supported phospholipid bilayer, Phys. Rev. Lett. 89 (2002).
[26] S.J. Johnson, T.M. Bayerl, D.C. McDermott, G.W. Adam, A.R. Rennie, R.K. Thomas, E. Sackmann, Structure of an adsorbed dimyristoylphosphatidylcholine bilayer measured with specular reflection of neutrons, Biophys. J. 59 (1991) 289–294.
[27] D.J. Muller, M. Kessler, F. Oesterhelt, C. Moller, D. Oesterhelt, H. Gaub, Stability of bacteriorhodopsin alpha-helices and loops analyzed by single-molecule force spectroscopy, Biophys. J. 83 (2002) 3578–3588.
[28] H. Luecke, B. Schobert, H.T. Richter, J.P. Cartailler, J.K. Lanyi, Structure of bacteriorhodopsin at 1.55 angstrom resolution, J. Mol. Biol. 291 (1999) 899–911.
[29] J.M. Cooper, J. Shen, F.M. Young, P. Connolly, J.R. Barker, G. Moores, The imaging of streptavidin and avidin using scanning tunnelling microscopy, J. Mater. Sci., Mater. Electron. 5 (1993) 106–110.
[30] J.A. Cappuccio, C.D. Blanchette, T.A. Sulchek, E.S. Arroyo, J.M. Kralj, A.K. Hinz, E.A. Kuhn, B.A. Chromy, B.W. Segelke, K.J. Rothschild, J. Fletcher, F. Katzen, T.C. Peterson, W.A. Kudlicki, G. Bench, P.D. Hoeprich, M.A. Coleman, Cell-free co-expression of functional membrane proteins and apolipoprotein forming soluble nanolipoprotein particles, Mol. Cell Proteomics (2008).
[31] F. Katzen, J.E. Fletcher, J.P. Yang, D. Kang, T.C. Peterson, J.A. Cappuccio, C.D. Blanchette, T. Sulchek, B.A. Chromy, P.D. Hoeprich, M.A. Coleman, W. Kudlicki, Insertion of membrane proteins into discoidal membranes using a cell-free protein expression approach, J. Proteome Res. 7 (2008) 3535–3542.
[32] W. Suhara, M. Kobayashi, H. Sagara, K. Hamada, T. Goto, I. Fujimoto, K. Torimitsu, K. Mikoshiba, Visualization of inositol 1,4,5-trisphosphate receptor by atomic force microscopy, Neurosci. Lett. 391 (2006) 102–107.
[33] R. Henderson, J.M. Baldwin, T.A. Ceska, F. Zemlin, E. Beckmann, K.H. Downing, Model for the structure of bacteriorhodopsin based on high-resolution electron cryomicroscopy, J. Mol. Biol. 213 (1990) 899–929.
[34] D.J. Muller, A. Engel, Atomic force microscopy and spectroscopy of native membrane proteins, Nat. Protocols 2 (2007) 2191–2197.
[35] I.G. Denisov, Y.V. Grinkova, A.A. Lazarides, S.G. Sligar, Directed self-assembly of monodisperse phospholipid bilayer nanodiscs with controlled size, J. Am. Chem. Soc. 126 (2004) 3477–3487.